ISPRS Journal of Photogrammetry and Remote Sensing 202 (2023) 1–12

Contents lists available at ScienceDirect

ISPRS Journal of Photogrammetry and Remote Sensing

journal homepage: www.elsevier.com/locate/isprsjprs

An assessment approach for pixel-based image composites

Saverio Francini [a,b,c,*], Txomin Hermosilla [d], Nicholas C. Coops [e], Michael A. Wulder [d], Joanne C. White [d], Gherardo Chirici [a,b]

[a] Department of Agriculture, Food, Environment and Forestry, Università degli Studi di Firenze. Via San Bonaventura, 13, 50145 Firenze, Italy
[b] Fondazione per il Futuro delle Città, Firenze, Italy
[c] NBFC, National Biodiversity Future Center, Palermo 90133, Italy
[d] Canadian Forest Service (Pacific Forestry Centre), Natural Resources Canada, 506 West Burnside Road, Victoria, British Columbia V8Z 1M5, Canada
[e] Integrated Remote Sensing Studio, Department of Forest Resources Management, University of British Columbia, 2424 Main Mall, Vancouver, British Columbia V6T 1Z4, Canada

ARTICLE INFO

Keywords:
Cloud-free composites
BAP
Medoid
Remote Sensing
Landsat

ABSTRACT

Remote sensing is one of the main sources of information for monitoring forest dynamics; however, surface reflectance is often not possible to accurately derive due to haze, cloud, or cloud shadow. Pixel-based composites are generated from multi-temporal images to cover the entire area of interest using several different methods. While the availability of free and open remote sensing data has further expanded the use of compositing approaches, to date a comprehensive methodology to assess the quality of these composites does not exist, nor is there a detailed set of compositing requirements to ensure consistent and reliable outputs to produce maps and statistics. Herein, we introduce a pixel-based composite assessment methodology based on five criteria: (i) number of valid observations and number of pixels with no available observations (data gaps), (ii) amount of unscreened clouds, cloud shadows, haze, or smoke (noise), (iii) radiometric consistency of the surface reflectance data, (iv) temporal proximity of pixels acquisition dates, and (v) spatial agreement of pixels acquisition dates. To test our methodology, we processed more than 16,000 Landsat images to generate and assess the Best Available Pixel (BAP) and the Medoid pixel-based composites for summer 2019 (2019-Jun-1 to 2019-Aug-31) over Europe, with a focus on the forested ecosystems. We found that BAP resulted in composites that were more temporally consistent, whereas the Medoid approach resulted in composites that were more radiometrically consistent.

Our results illustrate that our assessment approach is effective for comprehensively assessing the quality of pixel-based composites and could be implemented when using composites to generate statistical estimates (i.e. forest area) and for assessing the performance of new compositing algorithms or for selecting an appropriate compositing approach for a specific application.

1. Introduction

Free and open access remote sensing images are a powerful data source (Wulder and Coops, 2014). The Landsat mission, with more than 40 years of consistent surface reflectance data (Markham et al., 2018; Wulder et al., 2012, 2019), represents a key dataset for monitoring forest dynamics (Wulder et al., 2022), which is crucial in the current context of climate change. Recently, cloud-computing platforms have drastically increased the capabilities to process and manage remotely sensed data (Gomes et al., 2020), facilitating a variety of high-impact applications including deforestation, drought, disaster assessment, food security, water management, climate monitoring, and environmental protection (Gorelick et al., 2017). These large amounts of open-access remote sensing data, combined with increased processing and storage capabilities, have led to a transition from analysis focused on satellite scenes (i.e. satellite's acquisition path/row) to analysis involving entire regions, countries, or even global applications via the use of pixel-based composites.

Pixel-based compositing methodologies aim to produce cloud-free images covering entire study areas using reflectance values of different images acquired within defined temporal windows. Time series of Landsat pixel-based composites enable the generation of spatial

* Corresponding author at: Department of Agriculture, Food, Environment and Forestry, Università degli Studi di Firenze. Via San Bonaventura, 13, 50145 Firenze, Italy.
E-mail address: saverio.francini@unifi.it (S. Francini).

https://doi.org/10.1016/j.isprsjprs.2023.06.002
Received 13 October 2022; Received in revised form 26 May 2023; Accepted 3 June 2023
Available online 8 June 2023

information characterizing land cover, land cover change, and forest structural attributes in a dynamic, transparent, systematic, repeatable, and spatially exhaustive manner (Hansen et al., 2013; White et al., 2014; Hermosilla et al., 2016). These Landsat pixel-based composites have been used for studying forest disturbance (Senf and Seidl, 2020; Francini et al. 2020; Hermosilla et al., 2019; White et al., 2017), to predict and map forest structure and aboveground biomass (Zald et al. 2016; Matasci et al., 2018a, b; Hawrylo et al., 2020; Martilei et al., 2020; Francini et al., 2022a), to produce statistically rigorous estimates of forest disturbance areas (Francini et al., 2021, 2022b), and to map land cover and land-use dynamics at continental and global scales (Potapov et al., 2022).

In these aforementioned and similar studies, the theoretically desired inputs are cloud-free imagery acquired on the desired date(s) and covering the entire study area. However, clouds, haze, and related shadows limit the number of available observations and can result in data gaps (i.e. pixels with no observations within a defined period) (Saarinen et al., 2018). Similarly, obscured observations related to unscreened clouds, cloud shadows, atmospheric haze, or smoke, can limit the operational utility of pixel-based composites when interested in capturing status or changes to the Earth's surface. In addition, the number of days between the target date used for compositing and the observations' acquisition dates should be minimized to ensure that, for example, the composite relates to specific phenological phases. The acquisition date is of utmost importance when pixel-based composites and derived maps are used as intermediate products to derive official statistics referring to specific periods (Francini et al., 2022a). Finally, the capability of pixel compositing algorithms to limit the number of donor images from which observations are selected is also relevant for improving the spatial congruency among pixels acquisition dates, phenological phases, and atmospheric conditions and limiting the possibility of changes occurring between different acquisition dates. In summary, the desired traits of pixel-based composites include (i) no data gaps, (ii) lack of atmospheric interference, (iii) radiometrically consistent surface reflectance data, (iv) proximity of pixels acquisition dates to the target date, and (v) spatial congruency of pixels' acquisition dates. Despite the increasing prevalence of pixel-based composites, a set of key criteria with which to assess the quality of pixel-based composites does not currently exist.

Some of the pixel-based compositing methodologies involve the calculation of general statistics (e.g., average, median, maximum) among selected available observations (Simonetti et al., 2021). Aggregating different observations this way results in image composites made of values that (i) do not refer to specific dates but rather represent a range of dates (Flood, 2013), (ii) include incomparable measures across seasons, (iii) are impacted by haze, clouds, or shadows not correctly masked (Foga et al., 2017). Moreover, those composites are made of pixels in which the relationship between band values is not preserved, as they result from the aggregation (e.g., the average or the median) of several images. This can negatively impact the calculation of photosynthetic activity indices (Flood, 2013). To address those issues, different pixel-based compositing approaches were developed, such as WELD (Roy et al., 2010), the phenology-adaptive image compositing technique (Frantz et al., 2017), the Best Available Pixel composite (BAP) (Griffiths et al. 2013; White et al., 2014) and the Medoid (Kennedy et al. 2018; Flood, 2013). BAP and Medoid approaches are commonly used in the literature and are good examples to test a composite assessment methodology, as Medoid should provide superior results when considering the reflectance criteria, whereas BAP should be superior when considering criteria related to image acquisition dates.

BAP enables the selection of optimal observations from those available based on a set of criteria including the proximity of the acquisition date to the target date and the distance to clouds or cloud shadows (White et al., 2014). Alternately, the Medoid compositing method implemented by Kennedy et al. (2018) populates the pixels with surface reflectance values as similar as possible to the band-wise median value, which is calculated from all available images within a defined temporal window. As a result, for both BAP and Medoid, each pixel in the composite originates from a single "image donor", and different pixels can have different image donors. Despite the relevance and the need for working with consistent and reliable image composites, a comprehensive, unique, and exhaustive methodology to analyze the quality of such products is not commonly articulated.

This study aims to address this need by (i) introducing a comprehensive methodology for the assessment of pixel-based image composites over forests; (ii) demonstrating the methodology by comparing BAP and Medoid pixel-based compositing techniques over European forests; and (iii) providing guidelines on the assessment of pixel-based composites, highlighting those factors that should be considered in the context of scientific and rigorous remote sensing applications for forest monitoring through analysis of pixel-based image composites. To do so, we introduce and analyze a set of criteria that should be considered and taken into account when constructing composites, proposing new compositing algorithms, and choosing composites for specific applications.

2. Materials

2.1. Study area

The study area is Europe – defined as the European Union plus enclosed countries - with about 1018 Mha of land of which about 38% or 387 Mha are covered by forests and represent the focus of this study. 46% of European forests are predominantly coniferous, 37% are predominantly broadleaved, and the rest are mixed forests (Forest Information System for Europe, 2020). An estimated 17% of Europe's forest area was disturbed by anthropogenic and natural disturbances between 1986 and 2016 (Senf and Seidl, 2020), most of which were stand replacing (Palahí et al., 2021). Indeed, deforestation (permanent forest removal) is almost absent in Europe (Eurostat, 2022), and these disturbances do not represent a change in land cover (i.e. from forest-non-forest). Increased windthrow, fires, and insect disturbances are expected to be the greatest threat to European forests under a changing climate (Forzieri et al., 2022). To stratify our analysis and results by latitude and longitude, we constructed a tessellation of 100 × 100 km analysis units or tiles and selected all units overlapping Europe's landmass. As a result, 741 tiles were obtained (Fig. 1).

2.2. Forest mask

Forest areas of Europe were identified using the JAXA global forest mask which was generated by classifying the global 25-m resolution PALSAR-2/PALSAR SAR mosaic such that strong and low backscatter pixels are assigned as "forest" and "non-forest", respectively. The accuracy of the JAXA global forest mask is 86%, assessed using in-situ photos and high-resolution optical satellite images (JAXA, 2016). To match the Landsat resolution, the JAXA mask was resampled to 30 m. Although the most recent JAXA forest mask refers to 2017, no substantial land cover changes over forests are expected in the subsequent years due to the aforementioned very low level of deforestation in Europe.

2.3. Landsat data

Candidate images for producing pixel-based annual composites representing the European summer conditions were selected from the Landsat data holdings as mirrored on Google Earth Engine. The dataset consists of Landsat 7 and Landsat 8 surface reflectance imagery (Collection 1-Tier 1 on Google Earth Engine) atmospherically corrected using LEDAPS (Wolfe et al., 2004) and LaSRC (Vermote et al., 2018), respectively.

The bands used in this study were the three visible bands (blue,

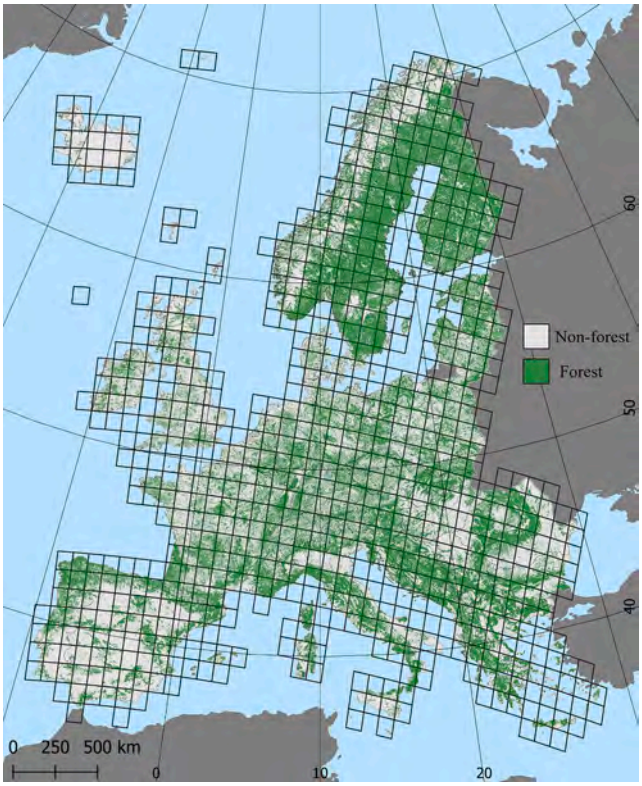

Fig. 1. Study area, the 741 100-km side tiles we used to stratify the analysis and the forest areas as identified by the JAXA forest mask.

green, and red), a near-infrared band (NIR), and two short-wave infrared bands (SWIR1, SWIR2) processed to orthorectified surface reflectance. These data include a mask generated using the C code based on the Function of Mask algorithm (CFMask, Foga et al. 2017) and informed on the presence of clouds, shadow, water, and snow. The candidate images used to construct cloud-free composites belong to the 578 Landsat scenes representing Europe with cloud cover $< 70\%$ (Vaglio et al., 2021, 2022). Images with cloud cover greater than this threshold are indeed more prone to geographical location errors, due to the challenges of performing geometric corrections when ground control points are obscured (Goward et al., 2017). Images acquired in 2018, 2019, and 2020 between June 01 and August 31 were used. The total number of Landsat images used in this study was 12,121: 3,943 for 2018, 4,281 for 2019, and 3,897 for 2020. Images acquired in 2018 and 2020 were used to identify and remove noise from composites of 2019 (see Section 3.3.2.), which was the actual year of assessment for the BAP and Medoid pixel-based composites.

2.4. Landsat reference data

To assess the radiometric consistency of BAP and Medoid composite surface reflectance data, we generated a reference dataset for July 2019, corresponding to the central month of the temporal window used to select imagery (June–August). Using a cloud threshold of 10%, 770 Landsat images were selected for the reference dataset, from which remaining clouds were masked out using the CFMASK algorithm (Foga et al., 2017). For those pixels where multiple images were available, the spectral values of the first image acquired were used as reference data. These selected images were removed from the compositing pool and are independent data that can be used for compositing assessment as indicated by White et al. (2014). Note that despite the cloud masking operation and the selection of imagery with low cloud cover, there is no guarantee that the reference values are flawless as some unscreened clouds or cloud shadows may be present. The total number of reference values was 2,118,825,742. No reference observations were available for 128 of our analysis tiles (Fig. 2). Considering tiles where at least a single reference observation was available, the average number of reference observations per tile was 3,456,486.

3. Methods

3.1. BAP algorithm

A comprehensive description of the logic and scoring rules for image compositing using the BAP approach introduced by Griffiths et al. (2013) and adapted by White et al. (2014), with key elements summarized in this section. Using the BAP, for each year and temporal window, the "best" observations from those available are selected based on four scoring functions which ranked observations based on: i) acquisition sensor, ii) proximity of acquisition date to the target date, iii) distance to cloud or cloud shadows, and iv) atmospheric opacity.

The sensor scoring function serves to mitigate the impact of spatial gaps associated with Landsat-7 ETM + SLC (Scan Line Corrector)-off data and to avoid spectral variability due to introducing multiple small image patches from the areas affected by the SLC-off. Thus, a lower sensor score is assigned to all observations acquired by Landsat 7 after 2003-May-31 (the date of failure of the SLC), while all observations belonging to Landsat 8 and Landsat 7 images acquired before 2003-May-31 receive the full sensor score.

Observations were also scored based on their acquisition date relative to the target Day Of Year (DOY). In this case, the target DOY was July 15, coinciding with the central date of the periods used for constructing the composite. Observations of images acquired closer to the target DOY were higher scored and so preferentially selected.

A distance to cloud or cloud shadow score was then assigned to each observation using the cloud masks produced for each Landsat image by the CFMASK algorithm. Pixels located at a distance greater than 1500 m from an identified cloud or cloud shadow pixel were assigned with the highest score. Pixels located<1500 m away from clouds and cloud shadows were assigned a weighted score following the function introduced in (Griffiths et al., 2013).

The atmospheric opacity band produced by LEDAPS is only available for Landsat 7. To accommodate the lack of opacity information, Landsat 8 observations are assumed to be clear and received the highest opacity score value (Hermosilla et al., 2019). For Landsat 7 the atmospheric opacity band was used to score the presence of haze and other atmospheric interferences. The highest score was assigned to observations with an opacity value < 0.2 while observations with an opacity value greater than 0.3 were excluded from the composting process. Observations with opacity values ≥ 0.2 and < 0.3 were labeled with a weighted score as per White et al. (2014).

3.2. Medoid calculation

Medoids are defined as "*representative objects of a data set or a cluster with a data set whose average dissimilarity to all the objects in the cluster is minimal*" (Struyf et al., 1997). The objective of the Medoid algorithm is to populate the final image composite pixels with the observation that has the most similar surface reflectance values to the median surface reflectance value calculated considering all images available but excluding clouds and shadows. Using the Medoid approach, the overall difference (in terms of Euclidean distance ED in the feature space) between images observations and the median of the entire time series (excluding pixels covered by clouds) defines the score that is used to select the optimum observations for compositing. As per the BAP approach, the Medoid compositing approach maintains the relationship between bands and produces composites in which observations refer to specific acquisition dates.

In this study, we used the method presented by Kennedy et al. (2018), which is an approximation of the medoid (Flood, 2013): first, for

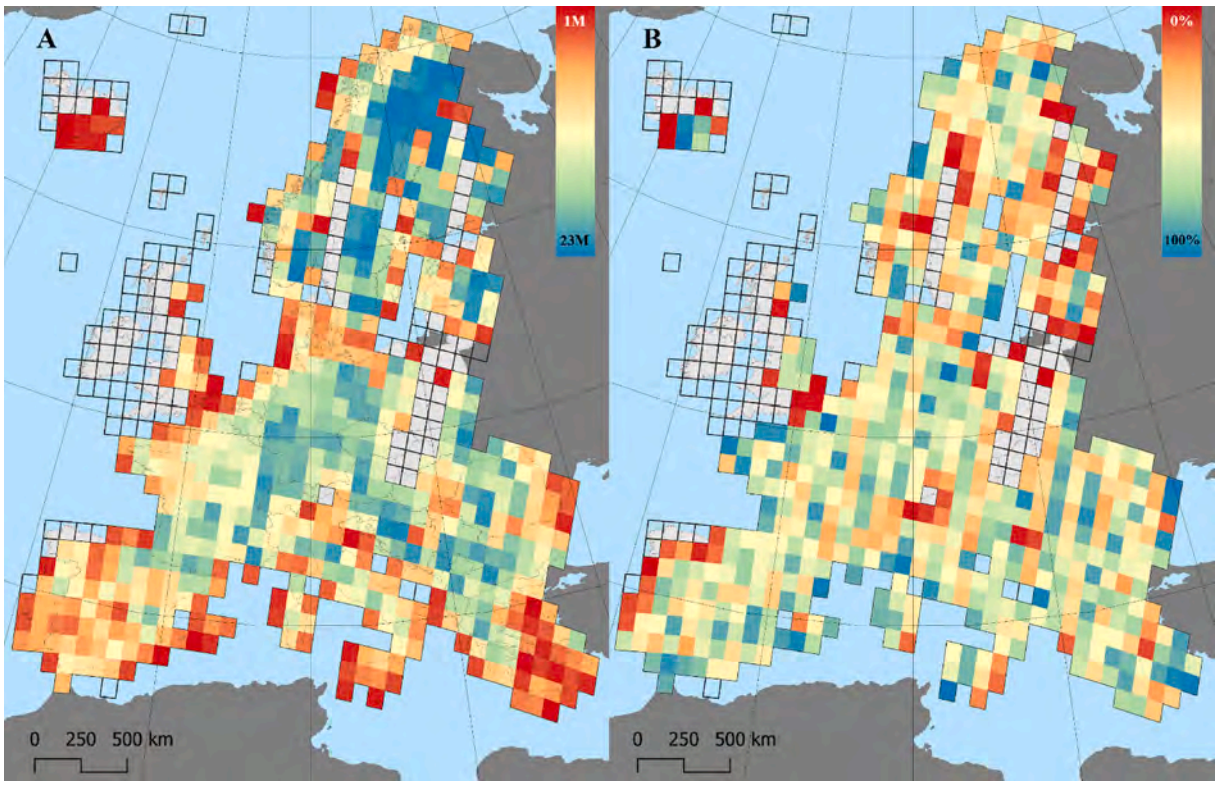

Fig. 2. Per-tile number of reference observations (A) and percentage within forested areas (B). Empty tiles had no reference observation.

each pixel and spectral band, the median value m is computed considering the entire image collection; then equation (1) is implemented to calculate for each pixel the ED.

$$\mathrm{ED} = \sum_{b=1}^{6} \sqrt{(m_b - i_b)^2} \quad (1)$$

Where b refers to the six Landsat bands considered, m is the pixel median value calculated in the first step, and i is the pixel value in the i^{th} image.

Finally, the band spectral values with the smaller ED are assigned to each output pixel. For the sake of comparability, pixel observations from Landsat 7 with an opacity value greater than 0.3 were a priori excluded from the analysis, as done for the BAP method. In those pixels with only two valid observations, the medoid value was given by randomly selecting one of the values.

3.3. Assessment of pixel-based composites

The assessment approach is based on five criteria: the number of per-pixel valid observations, the amount of noise, the radiometric consistency of the surface reflectance data, the temporal proximity of the pixel's acquisition date to the compositing target date, and the spatial agreement of pixel acquisition dates.

3.3.1. Valid observations and data gaps

The number of per-pixel valid observations indicates, for each pixel in the composite, the number of pixel observations not obscured by clouds, considering acquisitions within the time window selected to construct the composites. This aspect depends on the satellite revisit rate, the number of satellites in the constellation, and cloud coverage, and will thus be the same for BAP and Medoid composites. The greater the number of valid observations the greater the availability of candidate observations and the greater the relevance of the compositing algorithms selection. When the number of valid observations is equal to 1, any compositing pixel selection process will produce the same result. When the number of valid observations is equal to 0 the resulting image composite will contain data gaps.

3.3.2. Amount of noise

Noisy observations of pixels over forests (i.e. unscreened clouds, cloud shadows, haze, or smoke) can result in spikes over a photosynthetic index time series and can be detected by using the despiking algorithm (Kennedy et al., 2010), which can be applied independently to the six Landsat spectral bands considered in this study (Hermosilla et al., 2015a). The despiking algorithm requires observations for the year pre and post-target year, resulting in the need to construct pixel-based composites for 2018 and 2020, while 2019 was the actual year of analysis.

Specifically, a pixel value was flagged as noise if (i) the surface reflectance value of the spike detected in that band is greater than 0.01, AND (ii) the difference between the spectral value under consideration (2019) and the average of previous and subsequent years (2018 and 2020) exceeded a despiking threshold (0.6) in half or more of the Landsat bands considered. Where the spike was calculated as the absolute difference between pixel values in 2019 and the average between 2018 and 2020. The percentage of despiked pixels relative to the total amount of forested pixels was calculated for each tile and considered as an index of the amount of noise in the original composites.

3.3.3. Radiometric consistency

To assess the radiometric consistency, BAP and Medoid surface reflectance values were compared with those available in the reference dataset (White et al., 2014). The comparison was performed in terms of ED based on all the spectral bands (Eq. (1). The smaller the ED the greater the radiometric consistency of the bands' reflectance values. For each tile in the study area with reference data available, we calculated and reported the average of the ED of the pixels included. Moreover, as suggested by White et al. (2014), we calculated for each band the Pearson's correlation coefficient r between BAP and Medoid reflectance

values and those of the reference dataset. This procedure permits assessing the per-band agreement with reference data and thus comparing the radiometric consistency between bands.

3.3.4. Temporal proximity

For each pixel and composite, we computed the DOY Deviation (DOYD) as the number of days between the DOY in which the donor image was acquired and the DOY corresponding to the middle day of the period used for constructing the composite (i.e. July 15). The smaller the DOYD the greater the proximity between composite observations acquisition dates and the middle day of the period defined for constructing the composite. Decreasing the average DOYD of composite is expected to reduce (i) the spectral variability of the image due to vegetation phenological changes (relevant for classification tasks), and (ii) change occurrence probability (relevant for change detection tasks and statistics production).

3.3.5. Spatial agreement of acquisition dates

Pixel-based composites with tight temporal proximity may result in composites using values belonging to several different images—even if acquired close to the target date. In contrast, pixel-based composites made by a limited number of images—and thereby also a limited number of dates—help to prevent variations in phenological phases, atmospheric conditions, and possible land cover changes that can occur among different acquisition dates. We assessed the spatial agreement of acquisition dates by calculating for each tile the standard deviation of the composite observations acquisition DOYs (DOYSD). The smaller the DOYSD, the lower the variance among composite acquisition dates and thus the greater the composite quality, according to this criteria. A DOYSD equal to 0 indicates that all reflectance values in the composite come from images acquired on a single date, which is often the most desirable output when constructing composites. The larger the DOYSD, the greater the variance among composite acquisition dates and thus the lower the composite quality.

3.4. Influence of the number of valid observations on the assessment criteria

To determine how the number of valid observations influences the resulting composites, and to analyze the effect of an increasing number of valid observations (Van doninck and Tuomisto, 2017), we calculated, for each tile, the Pearson correlation coefficient *r* between the number of valid observations and the other four composite assessment criteria: the amount of noise, radiometric consistency, temporal proximity, and spatial agreement of composite acquisition dates.

4. Results

The number of valid observations per pixel ranged between 0 and 36 (Fig. 3). Generally, more observations were available in the south of Europe (e.g., Spain, Portugal, Italy), but several observations were also available in northern areas with low cloud cover during summer (e.g., Sweden, Finland), also due to the large overlap of paths in northern latitudes. Data gaps (i.e., pixels with no available observations) were extremely rare (1.1% in 2018, 0.9% in 2019, and 1.3% in 2020), and were mostly concentrated in Ireland, United Kingdom, and Iceland.

The percentage of noisy forested pixels was 10.2% for BAP and 6.8% for Medoid. Medoid noise was at least 10% smaller than BAP in 77% of tiles, was similar (±10%) in 13% of tiles, and was less for BAP than in 11% of tiles. The distribution of noise across Europe was very similar in BAP and Medoid composites (Fig. 4).

Regarding the radiometric consistency assessment, we found that the ED of the Medoid composite was generally lower than that produced with the BAP algorithm (on average −18% or 117 versus 139, in terms of surface reflectance). Analyzing the ED values at the tile level (Fig. 5), the Medoid composite had slightly smaller ED values than BAP and was thus more radiometrically consistent. Medoid ED was at least 10% smaller than BAP ED in 64% of tiles, was similar (ΔED ± 10%) in 28% of tiles, and was at least 10% smaller for BAP than Medoid in 7% of tiles.

The analysis of the agreement in surface reflectance values between BAP and Medoid composites with reference values indicated a greater agreement of Medoid bands than BAP (Fig. 6). On average, Pearson correlation coefficient values were always equal to or greater than 0.65, suggesting strong spectral agreement for both BAP and Medoid.

Concerning temporal proximity (Fig. 7), the DOYD average was 18 days for the BAP and 24 days for the Medoid. DOYD was at least 10% smaller for BAP than Medoid in 51% of pixels, was similar (±10%) in 29% of pixels, and was at least 10% smaller for Medoid than BAP in 20% of pixels. Fig. 7 shows very different patterns between BAP and Medoid acquisition dates. BAP composite has large areas of pixel values acquired on the same day, while the number of adjacent pixels acquired on the same day was consistently smaller in the Medoid composite.

The spatial agreement of pixel values acquisition dates assessment indicated DOYSD values ranging between 0 and 25 in both BAP and

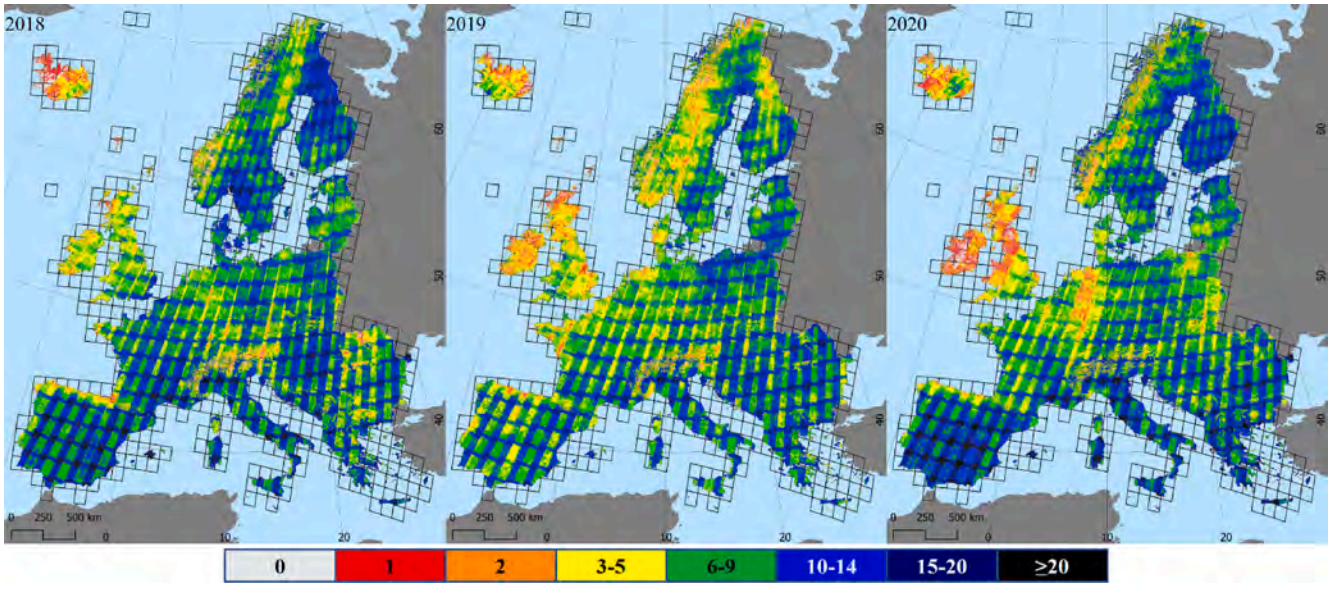

Fig. 3. Number of per-pixel valid observations per analysis tile.

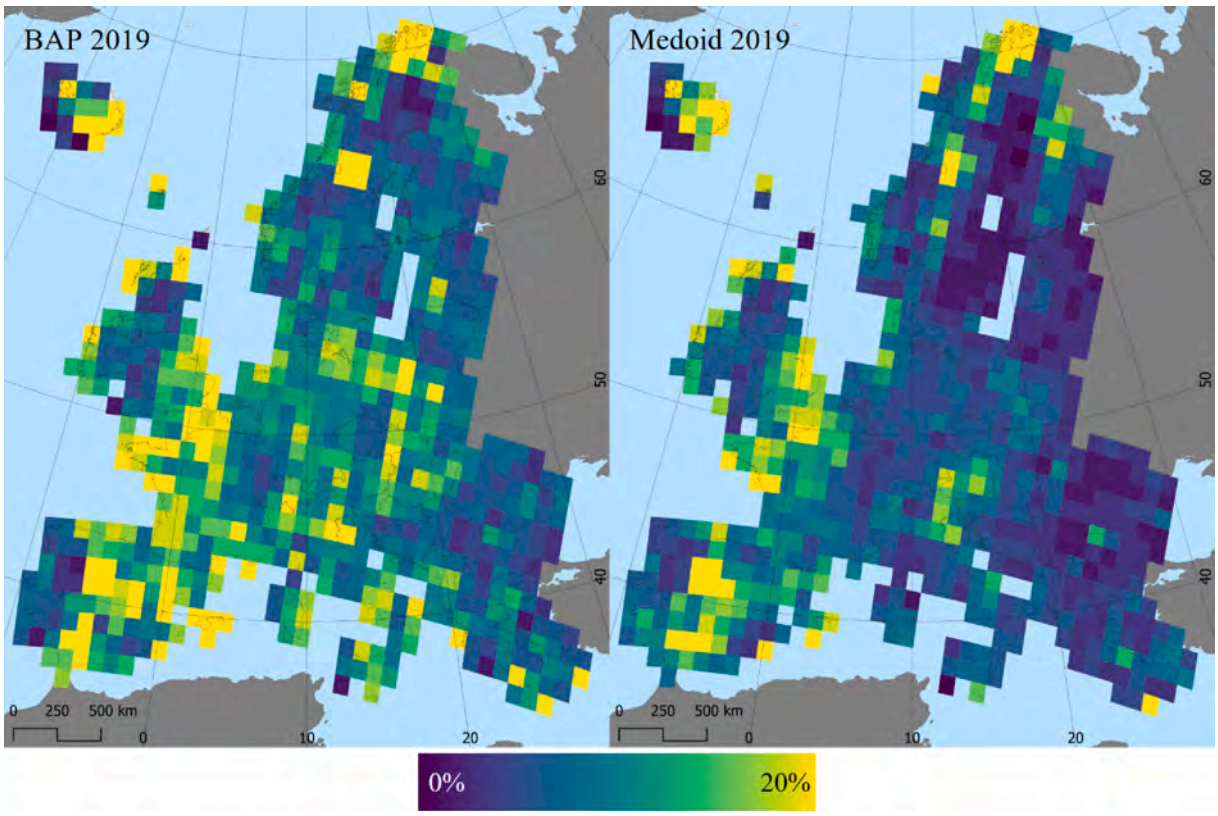

Fig. 4. Per-tile percentage of noisy pixels relative to the total number of forested pixels in each 100 km analysis tile.

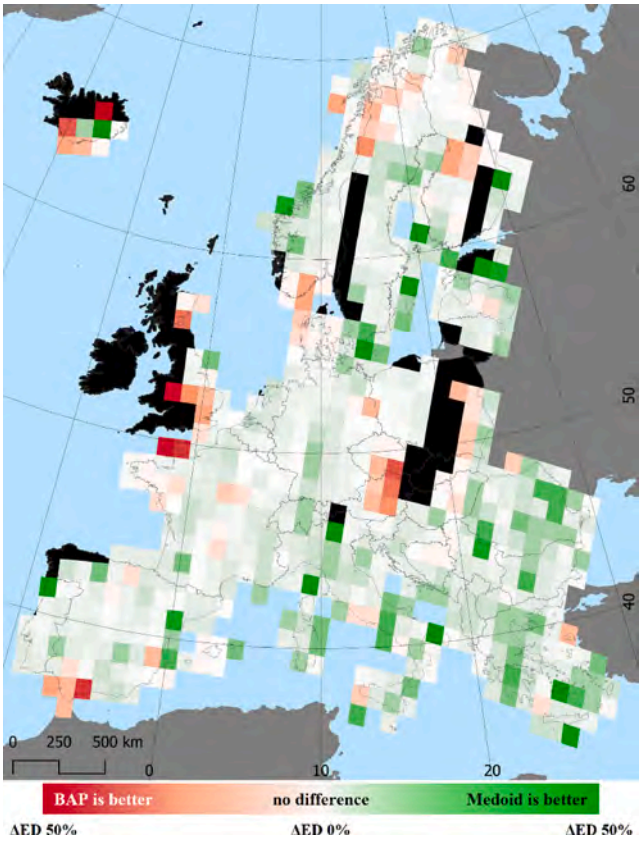

Fig. 5. Per-tile BAP and Medoid Euclidean distance (ED) comparison.

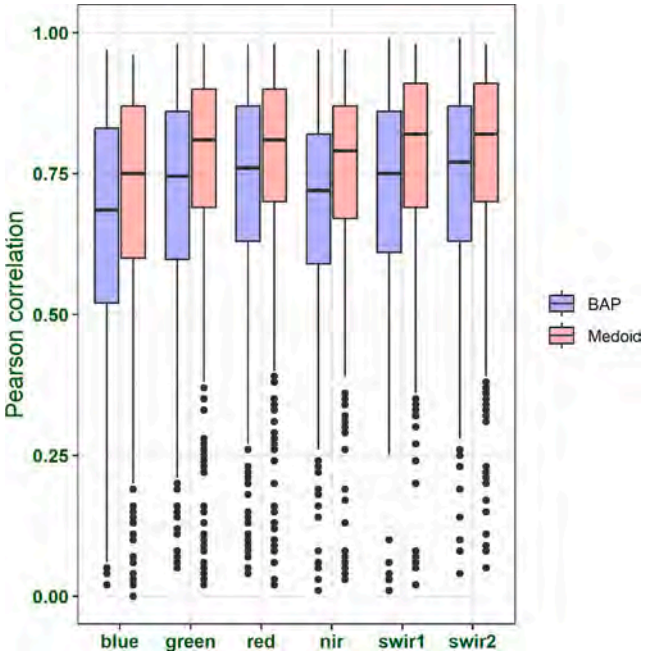

Fig. 6. Box plot of the Pearson correlation coefficient r values between BAP and Medoid composite bands and reference values calculated for each tile.

Medoid composites (Fig. 8). DOYSD was at least 10% smaller for the BAP than Medoid in 84% of tiles, was similar (±10%) in 14% of tiles, and was smaller for the Medoid than BAP by at least 10% in 2% of tiles.

In Fig. 9 we summarize the outcomes of the composites assessments performed which produce different and comparable results for BAP and Medoid.

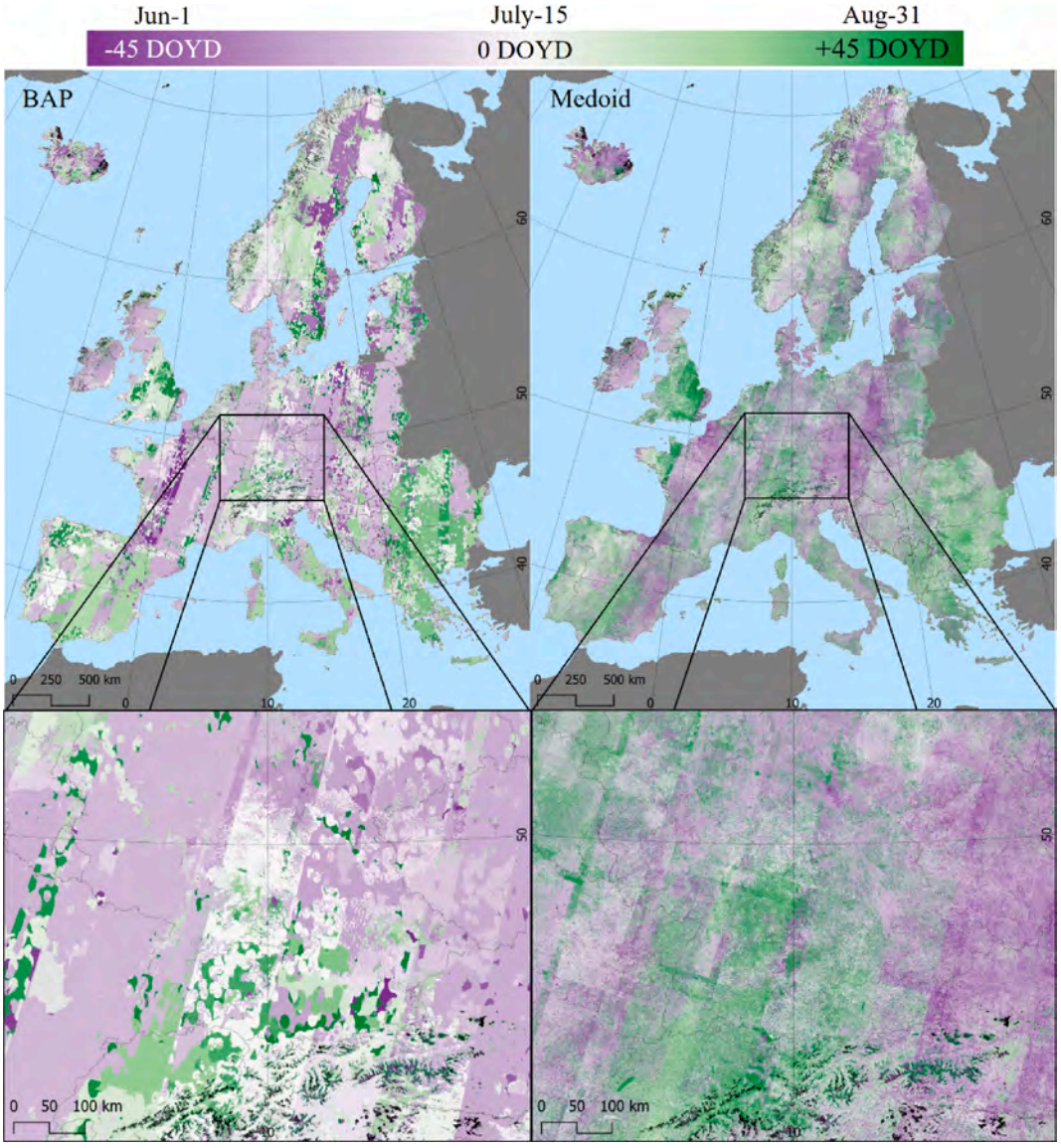

Fig. 7. The temporal proximity of BAP and Medoid composites. The smaller the DOYD (day of interest deviation) – and the lighter the colors - the smaller the distance (in days) between acquisition DOYs and the middle day of the time window used for constructing the composite (July 15), and thus the greater the temporal proximity of the composite.

Finally, Fig. 10 shows scatter plots (panels A-D) - and the resulting Pearson correlation coefficient values (panel I) - between the number of valid observations for the tile and the other four composite assessment criteria. Results indicated negative agreement between the number of valid observations and noise, ED, and DOYD. The strongest positive agreement was found between the number of valid observations and DOYSD, with Pearson correlation coefficient r of 0.46 for BAP and 0.66 for Medoid.

5. Discussion

5.1. Contextualization of the study

Several remote sensing applications require the construction of pixel-based image composites such as BAP and Medoid, which aim to produce a single image approximation of the whole study area under ideal atmospheric conditions by combining multiple images based on given compositing rules and relying on automatic cloud detection methods. The selection of the compositing algorithm and rules, as well as the presence of atmospheric interferences—both seasonal and permanent—results in image composites with different levels of quality. However, pixel-based composites should meet specific requirements, as they are often used to produce official statistics (FAO, 2020) and to monitor forest disturbance (Francini et al., 2022b), and recovery (Pérez-Cabello et al., 2021; Viana-Soto et al., 2020), classify land cover (Alam et al., 2020), and predict (Cavalli et al., 2022, 2023) and quantify afforestation areas (Francini et al., 2023).

In this study, we introduced a methodology for the assessment of pixel-based Landsat composites. We demonstrated our approach by assessing BAP and Medoid composites over European forests based on five main requirements or criteria: data gaps, noise, radiometric consistency, temporal proximity, and spatial agreement of acquisition dates. To test our approach, we processed 16,481 Landsat images and constructed BAP and Medoid pixel-based composites referring to 2018, 2019, and 2020 summer conditions (June-August). 2019 was the actual year of analysis, while 2018 and 2020 composites were constructed to enable the detection of noisy observations in the 2019 composite (Hermosilla et al., 2015a, Kennedy et al., 2010).

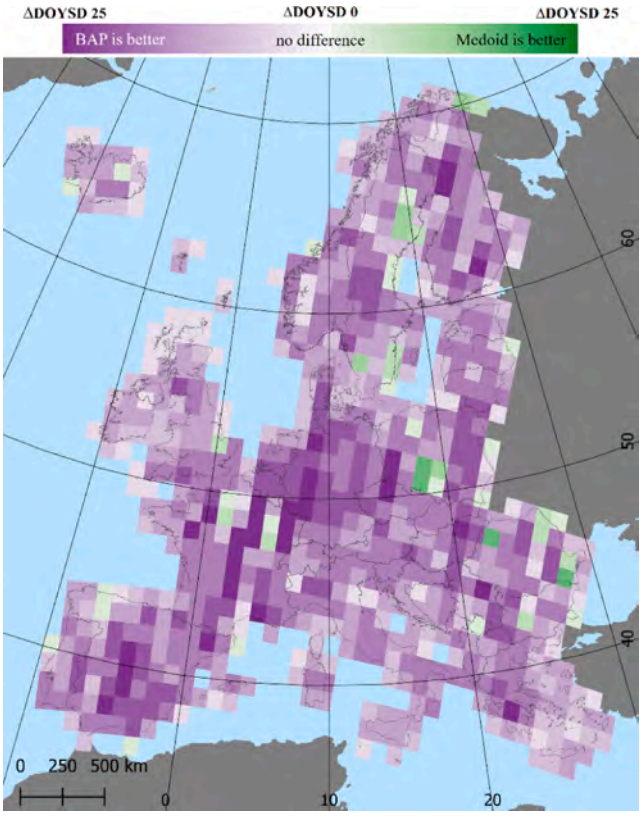

Fig. 8. *Absolute difference between BAP and Medoid composites* DOYSD.

5.2. Number of valid observations and data gaps

Data gaps are traditionally a quality aspect of primary importance for composites (Chen et al., 2011), and for this reason, multiple studies have developed methods to address these data gaps (Siabi et al., 2022; Lan et al., 2022). The number of gaps does not depend on the compositing algorithms but rather on the availability of cloud-free observations dictated by sensor revisit time and regional cloud coverage. In contrast, the amount of noise, radiometric consistency, temporal proximity, and the spatial agreement of acquisition dates are strongly related to the compositing algorithms used. In assessing data gaps, we found very large variability in the amount of Landsat data available across Europe (Fig. 3). While for some pixels no Landsat observations were available for the 2018–2020 period, some pixels had up to 36 observations, confirming the need for appropriate pixel values selection processes. The average amount of data gaps in the 2018–2020 period was 1.1%.

5.3. Amount of noise

The despiking procedure we applied (Kennedy et al., 2010; Hermosilla et al., 2015a) quantifies the amount of noise in the composites. When focusing the analysis on forests - which were the target of our study - the despiking algorithm represents a powerful tool that helps to remove any possible remaining noise from composites. To analyze pixels in which land cover changes are not expected to occur, and thus to properly assess the five criteria we introduced, the focus of this study was on forests, as deforestation is almost absent in Europe (Palahí et al., 2021), and as active forest management affects a small proportion of the total area. Depending on the analysis, the despiking threshold calibration may be very important (Chirici et al., 2020) as, for example, forest disturbance followed by rapid forest recovery can be detected as noise (Francini et al., 2021). When image composites are used for classification, noise in the composites may result in labeling errors, whereas when image composites are used in regression-based approaches, noise may result in the prediction of outliers. Although the despiking algorithm used herein represents a well-established approach for removing noise from composites (Kennedy et al., 2018, 2010), and although it was further improved by Hermosilla et al. (2019), it should be noted that it is not without error, and therefore that the amount of noise identified is only an estimate. However, the error associated with the despiking process is expected to be similar for each composite (i.e. Medoid and BAP) and therefore the algorithm provides estimates of the amount of noise, which are comparable across different composites and which can be calculated across large areas. In our experiments, the amount of noise relative to forested pixels in our analysis tiles was larger for BAP than for Medoid (an average of + 3.7%), because the Medoid pixel selection process focuses on maximizing the radiometric consistency of surface reflectance data, while BAP considers different criteria.

5.4. Radiometric consistency

The Euclidean distance represents a useful summary statistic for assessing the radiometric consistency (White et al., 2014; Griffiths et al., 2013) of multi-band imagery. While calculating the correlation coefficient between reference data and pixel-based composites returns one result for each band, the Euclidean distance characterizes the overall radiometric consistency for all bands with a single value. For an example of the operational application of the ED criteria, we can consider a composite designed to detect pest attacks in forest ecosystems. In this case, if the ED between a pest-affected forest and a healthy forest is known and equal to *A*, and if the radiometric consistency in terms of ED of the pixel-based image composite is *B*, then the composite will be of little use if *A* and *B* are in the same order of magnitude, but it will be definitely useful if *A* is one or two orders of magnitude greater than *B*.

In this study, Euclidean distance served as an efficient parameter to measure the spectral similarity between composites and reference

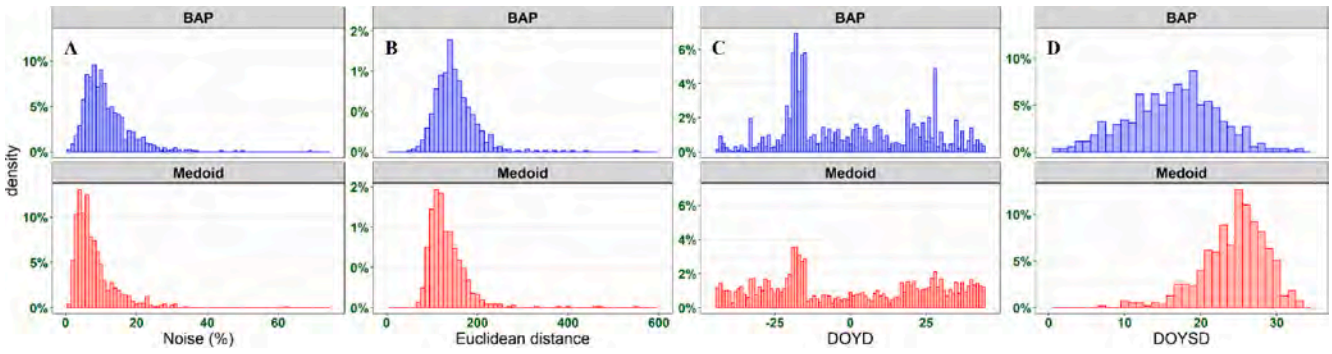

Fig. 9. Density histograms resulting from the assessments of BAP and Medoid composites: the amount of noise (A), the radiometric consistency (B), the temporal proximity (C), and the spatial agreement of acquisition dates (D).

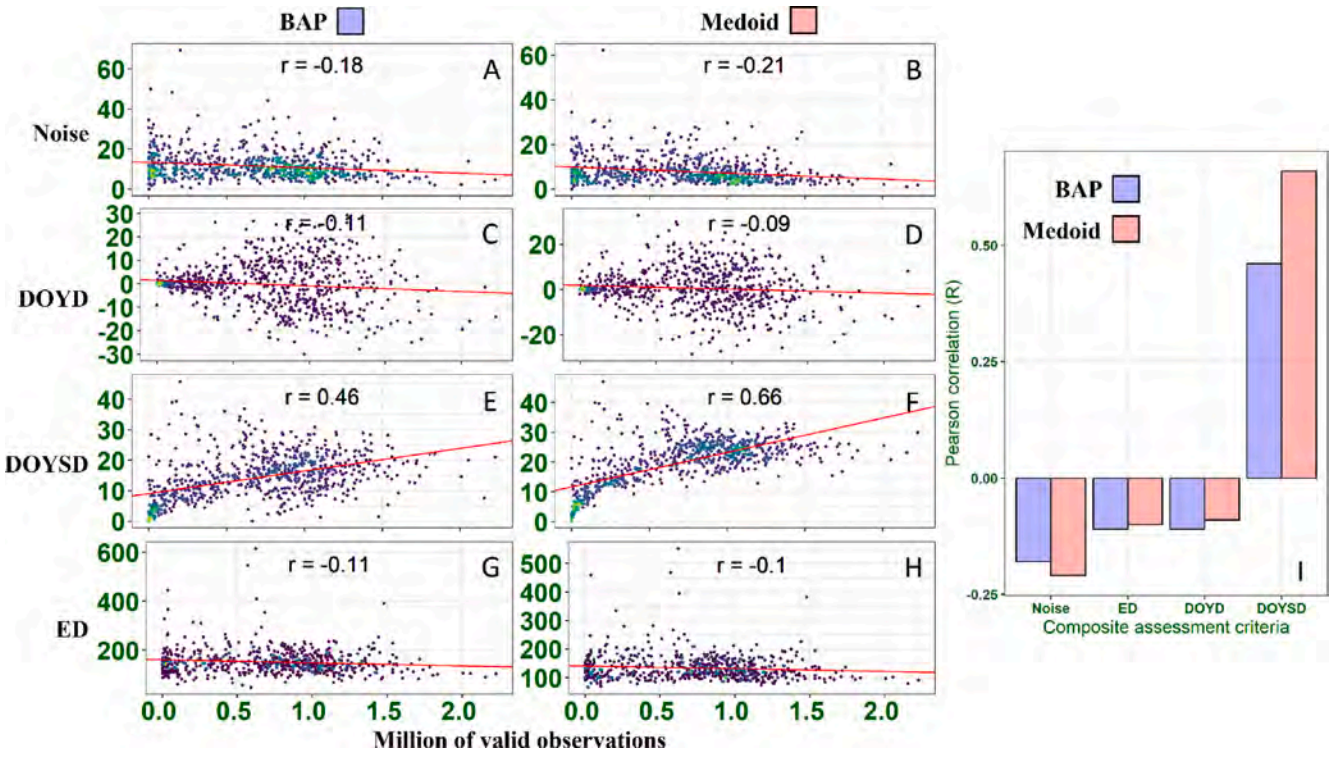

Fig. 10. Panels A-H show BAP and Medoid scatter plots between the total number of valid observations over forested pixels (section 3.3.1) and Noise (section 3.3.2), ED (section 3.3.3), DOYD (section 3.3.4), and DOYSD (section 3.3.5). Panel I shows a summary of the Pearson correlation coefficient values.

values, as the smaller the Euclidean distance the greater the similarity between the composites and the reference Landsat observations. At the European level (Fig. 5), Euclidean distance was 18% smaller for Medoid. At the tile level, Euclidean distance was consistently (difference greater than 10%) smaller for Medoid in 64% of our analysis tiles. The assessment of the spectral agreement resulted in large values for both BAP (r = 0.65–73) and Medoid (r = 0.7–0.77), indicating strong correspondence with reference values, in particular considering that the agreement was assessed between values belonging to imagery acquired over different dates and thus with possible existing subtle variations in the phenological phase and environmental conditions. As a result, the spectral agreement computed using Pearson correlation coefficient *r* suggests that both Medoid and BAP approaches allowed for the generation of composites whose spectral reflectance values were reliable and radiometrically consistent. Finally, the analysis of the agreement between the number of valid observations and composite assessment criteria suggested that more valid observations result in an improvement of the radiometric consistency as both noise and ED are reduced, as well as an enhancement of the temporal proximity as the DOYD decreases.

5.5. *Temporal proximity*

Temporal proximity, according to the herein presented methodology, is one of the requirements of the pixel-based composite that needs attention and specific assessment. Temporal proximity is a key feature in meaningfully defining composite acquisition dates and can be particularly relevant when maps derived from pixel-based composites are used as intermediate products to generate statistics (Testa et al., 2014; Zeng et al., 2021). Pixel-based composites should indeed have spectral values referring as much as possible to the target date they are intended to represent (Hagolle et al., 2005). Pixel-based composites referring as much as possible to a specific day or period are crucial to (i) defining the period over which we are producing forest disturbance area estimates (Francini et al., 2022a) and (ii) limiting the phenological variation. This second aspect is crucial, for example, in forest disturbance detection via analysis of annual composites time series (Hermosilla et al., 2015b; Kennedy et al., 2010). In such applications, disturbed pixels are discriminated from undisturbed or stable forest pixels in which the photosynthetic activity has not changed through time. The analysis of annual time series based on pixel-based composites using values belonging to imagery acquired far away from the target day of the year may lead to the incorrect detection of changes that are attributable to differences in photosynthetic activity due to differences in phenology. While phenological differences could be minimized also by reducing the time window used to select the imagery, this would result in an increment of data gaps, as fewer images would be available for providing values to construct the composite. Accordingly, in this study, we used a three-month time window to select candidate imagery (June to August), which still resulted in ~1% of pixels with no valid observations and ~15% of pixels with less than five valid observations over Europe. For an additional example of the operational application of the temporal proximity criteria, we can consider a composite designed to detect drought. Droguth forest disturbances are characterized by a short duration and they are clearly visible in remote sensing imagery just for a short period, which makes key to exploit composites with optimal temporal proximity in these cases. For example, if the study case is a drought forest disturbance that is expected to be clearly visible in the first two weeks of August, the ideal pixel-based composite should be constructed using August 7 as the target date and should have a DOYD smaller or equal to 7.

The temporal proximity assessment we performed highlighted large differences between BAP and Medoid compositing algorithms' pixel values selection processes. Whereas Medoid considered the band's reflectance to perform the observations selection process and obtained results were slightly better in terms of noise and Euclidean distance, BAP observations selection considered the acquisition dates and enabled the construction of composites that were more reliable in terms of temporal proximity and the spatial agreement of acquisition dates. Temporal proximity is measured in DOYD and was, on average, about 6 days less for BAP than Medoid (Fig. 7). This means that with respect to Medoid,

BAP composite values tend to be acquired nearer by about 6 days to the target day of year used to construct the composite. In other words, the BAP approach tends to select observations from a narrower date range. This characteristic is particularly relevant when several subsequent composites referring to different periods are needed (Coops et al., 2022). If they have large DOYDs, the difference between their acquisition dates is maximized. Alternately, if they have small DOYDs, there may be overlapping observations, such that different composites have more values belonging to imagery acquired on the same dates.

5.6. Spatial agreement of acquisition dates

The fifth and last composite assessment criteria we introduced in this study is the DOY Standard Deviation (DOYSD). Smaller DOYSD values indicate less variance among composite acquisition dates and thus less expected changes and higher composite quality. For an example of the operational application of the spatial agreement of acquisition dates criteria, we can consider a composite designed to perform an image segmentation task. The smaller the DOYSD, the smaller the number of images and dates considered to construct the composite, and thus the smaller the expected changes among composite observations in phenological phases, atmospheric conditions and the smaller the occurrence probability of land cover changes. These are all composite key features to perform segmentation tasks and can be assessed through the DOYSD.

In this study, DOYSD was smaller for BAP than Medoid in almost all of our analysis tiles (Fig. 8), meaning that BAP tends to construct composites whose values came from a smaller range of acquisition dates. This behavior helps to decrease the spatial variability between different acquisitions and reduces possible atmospheric condition changes, which complicate data extrapolation by model prediction and negatively impact classification task accuracies (Tuia et al., 2016). The capability of BAP in creating composites with small DOYSD can be related to (i) sensor and (ii) DOY scores (Section 3.1), which are attributed to whole images and not single pixels, facilitating thus the selection or the removal of entire portions of images in the final composite. The number of valid observations has a strong positive correlation with DOYSD (Fig. 10E, F), consistently larger than with other criteria, indicating that more valid observations relevantly increase the DOYSD and thus decrease the spatial agreement of pixel values' acquisition dates, as the more valid observations from which the compositing algorithm can choose, the greater the chance to select pixels values and the difficult the selection process.

5.7. Future perspectives

Overall, the capacity to quantitatively assess the quality and illuminate the differences between different pixel-based compositing approaches aids in understanding the suitability of the derived image composites for their intended application (White et al., 2014). Herein, we have a special focus on forest statistics reporting requirements (e.g., total forest area, total forest area disturbed) and therefore highlight those criteria that are most relevant to deriving mapped outcomes and associated statistics. In this context, our analysis and results indicate that the BAP approach is preferable for applications in which temporally constrained composites are needed. This can be crucial when images are used to produce statistics for specific periods, or image segmentation. Differently, Medoid may be the first choice if the application needs radiometrically consistent composites and more simple pre-processing procedures. However, depending on the intended purpose of the mapping activity, the relevance of composite assessment criteria may change. Critically, our analysis indicates that both the BAP and Medoid compositing approaches generate composites that are radiometrically consistent, which is ultimately a key requirement for any application. The composite quality criteria introduced in this study aim to identify the strengths and weaknesses of pixel-based image composites for forest monitoring applications. The ultimate decision, however, regarding which compositing approach to use must be based on the objectives of the mapping activity for which the composite will be used. In addition, other non-forest ecosystems may have different information needs and alternate image composite assessment criteria should be investigated. Newly developed compositing approaches can likewise be assessed following a similar approach and criteria and the results herein provide a useful baseline for understanding algorithmic advances in compositing and opportunities for improvement.

6. Conclusion

Herein, we presented a new approach for the quality assessment of pixel-based image composites according to five key composite criteria: number of valid observations and data gaps, amount of noise, radiometric consistency, temporal proximity, and spatial agreement of acquisition dates. We processed more than 16,000 Landsat images and applied our assessment approach to quantitatively and objectively compare BAP and Medoid composites over European forests. The approach presented is rigorous yet readily implemented and is adaptable to different data sources. Such quality assessments of image composites are critical when composites are used to derive mapped outcomes and statistics for reporting purposes, and can also be useful for transparent assessment when new compositing methodologies are introduced.

Declaration of Competing Interest

The authors declare that they have no known competing financial interests or personal relationships that could have appeared to influence the work reported in this paper.

Acknowlegments

This study was supported by the following projects: 1. MULTIFOR "Multi-scale observations to predict Forest response to pollution and climate change" PRIN 2020 Research Project of National Relevance funded by the Italian Ministry of University and Research (prot. 2020E52THS); 2. SUPERB "Systemic solutions for upscaling of urgent ecosystem restoration for forest related biodiversity and ecosystem services" H2020 project funded by the European Commission, number 101036849 call LC-GD-7-1-2020; 3. EFINET "European Forest Information Network" funded by the European Forest Institute, Network Fund G-01-2021. 4. FORWARDS: the forestward observatory to secure resilience of european forests (Project 101084481). 5. PNRR, funded by the Italian Ministry of University and Research, Missione 4 Componente 2, "Dalla ricerca all'impresa", Investimento 1.4, Project CN00000033.

References

Alam, A., Bhat, M.S., Maheen, M., 2020. Using Landsat satellite data for assessing the land use and land cover change in Kashmir valley. GeoJournal 85, 1529–1543. https://doi.org/10.1007/s10708-019-10037-x.

Cavalli, A., Francini, S., Cecili, G., Cocozza, C., Congedo, L., Falanga, V., Spadoni, G.L., Maesano, M., Munafò, M., Chirici, G., Scarascia Mugnozza, G., 2022. Afforestation monitoring through automatic analysis of 36-years Landsat Best Available. Composites iForest 15, 220–228. https://doi.org/10.3832/ifor4043-015.

Cavalli, A., Francini, S., McRoberts, R.E., Falanga, V., Congedo, L., De Fioravante, P., Maesano, M., Munafò, M., Chirici, G., Scarascia, M.G., 2023. Estimating Afforestation Area Using Landsat Time Series and Photointerpreted Datasets. Remote Sens. (Basel) 15 (4), 923. https://doi.org/10.3390/rs15040923.

Chen, J., Zhu, X., Vogelmann, E.J., Gao, F., Jin, S., 2011. A simple and effective method for filling gaps in Landsat ETM+ SLC-off images. Remote Sens. Environ. 1015, 1053–1064. https://doi.org/10.1016/j.rse.2010.12.010.

Chirici, G., Giannetti, F., Mazza, E., et al., 2020. Monitoring clearcutting and subsequent rapid recovery in Mediterranean coppice forests with Landsat time series. Ann. For. Sci. 77, 40. https://doi.org/10.1007/s13595-020-00936-2.

Coops, C.N., Tompalski, P., Goodbody, R.H.T., Achim, A., Mulverhill, C., 2022. Framework for near real-time forest inventory using multi source remote sensing data. Forestry: An International Journal of Forest Research cpac015. https://doi.org/10.1093/forestry/cpac015.

Deforestation: causes and how the EU is tackling it. 2022. Eurostat. https://ec.europa.eu/eurostat.

Flood, N., 2013. Seasonal Composite Landsat TM/ETM+ Images Using the Medoid (a Multi-Dimensional Median). Remote Sens. (Basel) 5 (12), 6481–6500. https://doi.org/10.3390/rs5126481.

Foga, S., Scaramuzza, P.L., Guo, S., Zhu, Z., Dilley, R.D., Beckmann, T., Schmidt, G.L., Dwyer, J.L., Hughes, M.J., Laue, B., 2017. Cloud detection algorithm comparison and validation for operational Landsat data products. Remote Sens. Environ. 194 https://doi.org/10.1016/j.rse.2017.03.026.

Food and Agriculture Organization of the United Nations. 2020. The state of the worlds's forests. https://www.fao.org/3/ca8642en/ca8642en.pdf.

Francini, S., McRoberts, R.E., Giannetti, F., Mencucci, M., Marchetti, M., Scarascia Mugnozza, G., Chirici, G., 2020. Near-real time forest change detection using PlanetScope imagery. Eur. J. Remote Sens. 53 (1), 233–244. https://doi.org/10.1080/22797254.2020.1806734.

Francini, S., McRoberts, R.E., Giannetti, F., Marchetti, M., Scarascia Mugnozza, G., Chirici, G., 2021. The Three Indices Three Dimensions (3I3D) algorithm: a new method for forest disturbance mapping and area estimation based on optical remotely sensed imagery. Int. J. Remote Sens. 42 (12), 4697–4715. https://doi.org/10.1080/01431161.2021.1899334.

Francini, S., D'Amico, G., Vangi, E., Borghi, C., Chirici, G., 2022. Integrating GEDI and Landsat: Spaceborne Lidar and Four Decades of Optical Imagery for the Analysis of Forest Disturbances and Biomass Changes in Italy. Sensors 22 (5), 2015. https://doi.org/10.3390/s22052015.

Francini, S., McRoberts, R.E., D'Amico, G., Coops, N.C., Hermosilla, T., White, J.C., Wulder, M.A., Marchetti, M., Mugnozza, G.S., Chirici, G., 2022b. An open science and open data approach for the statistically robust estimation of forest disturbance areas. Int. J. Appl. Earth Obs. Geoinf. 106, 102663.

Forzieri, G., Dakos, V., McDowell, N.G., et al., 2022. Emerging signals of declining forest resilience under climate change. Nature 608, 534–539. https://doi.org/10.1038/s41586-022-04959-9.

Francini, S., Cavalli, A., D'Amico, G., McRoberts, R.E., Maesano, M., Munafò, M., Scarascia Mugnozza, G., Chirici, G., 2023. Reusing Remote Sensing-Based Validation Data: Comparing Direct and Indirect Approaches for Afforestation Monitoring. Remote Sens. (Basel) 15 (6), 1638. https://doi.org/10.3390/rs15061638.

Frantz, D., Röder, A., Stellmes, M., Hill, J., 2017. Phenology-adaptive pixel-based compositing using optical earth observation imagery. Remote Sens. Environ. 190, 331–347.

Gomes, V.C.F., Queiroz, G.R., Ferreira, K.R., 2020. An Overview of Platforms for Big Earth Observation Data Management and Analysis. Remote Sens. 12, 1253. https://doi.org/10.3390/rs12081253.

Gorelick, N., Hancher, M., Dixon, M., Ilyushchenko, S., Thau, D., Moore, R., 2017. Google Earth Engine: Planetary-scale geospatial analysis for everyone. Remote Sens. Environ. 202, 18–27. https://doi.org/10.1016/j.rse.2017.06.031.

Goward, S.N., Williams, D.L., Arvidson, T., Rocchio, L.E.P., Irons, J.R., Russell, C.A., Johnston, S.S., 2017. Landsat's Enduring Legacy: Pioneering Global Land Observations from Space. American Society for Photogrammetry and Remote Sensing, Bethesda, MD.

Griffiths, P., van der Linden, S., Kuemmerle, T., Hostert, P., 2013. A pixel-based Landsat compositing algorithm for large area land cover mapping. Journal of Selected Topics in Applied Earth Observations and Remote Sensing 6 (5), 2088–2101.

Hagolle, O., Lobo, A., Maisongrande, P., Cabot, F., Duchemin, B., De Pereyra, A., 2005. Quality assessment and improvement of temporally composited products of remotely sensed imagery by combination of VEGETATION 1 and 2 images. Remote Sens. Environ. https://doi.org/10.1016/j.rse.2004.09.008.

Hansen, M.C., Potapov, P.V., Moore, R., Hancher, M., Turubanova, S.A., Tyukavina, A., 2013. High-Resolution Global Maps of 21st-Century Forest Cover Change. Science (80-.). 342, 850–854.

Hawryło, P., Francini, S., Chirici, G., Giannetti, F., Parkitna, K., Krok, G., Mitelsztedt, K., Lisańczuk, M., Stereńczak, K., Ciesielski, M., Wężyk, P., Socha, J., 2020. The Use of Remotely Sensed Data and Polish NFI Plots for Prediction of Growing Stock Volume Using Different Predictive Methods. Remote Sens. (Basel) 12 (20), 3331. https://doi.org/10.3390/rs12203331.

Hermosilla, T., Wulder, M.A., White, J.C., Coops, N.C., Hobart, G.W., 2015a. An integrated Landsat time series protocol for change detection and generation of annual gap-free surface reflectance composites. Remote Sens. Environ. 158, 220–234. https://doi.org/10.1016/j.rse.2014.11.005.

Hermosilla, T., Wulder, M.A., White, J.C., Coops, N.C., Hobart, G.W., 2015b. Regional detection, characterization, and attribution of annual forest change from 1984 to 2012 using Landsat-derived time-series metrics. Remote Sens. Environ. 170, 121–132. https://doi.org/10.1016/j.rse.2015.09.004.

Hermosilla, T., Wulder, M.A., White, J.C., Coops, N.C., Hobart, G.W., Campbell, L.B., 2016. Mass data processing of time series Landsat imagery: pixels to data products for forest monitoring. Int. J. Digit. Earth 9, 1035–1054. https://doi.org/10.1080/17538947.2016.1187673.

Hermosilla, T., Wulder, M.A., White, J.C., Coops, N.C., 2019. Prevalence of multiple forest disturbances and impact on vegetation regrowth from interannual Landsat time series (1985–2015). Remote Sens. Environ. 233, 111403 https://doi.org/10.1016/j.rse.2019.111403.

JAXA, 2016. Global 25m Resolution PALSAR-2 / PALSAR Mosaic and Forest / Non-Forest Map (FNF) Dataset Description Japan Aerospace Exploration Agency (JAXA) Earth Observation Research Center (EORC).

Kennedy, R.E., Yang, Z., Cohen, W.B., 2010. Detecting trends in forest disturbance and recovery using yearly Landsat time series: 1. LandTrendr - Temporal segmentation algorithms. Remote Sens. Environ. 114, 2897–2910. https://doi.org/10.1016/j.rse.2010.07.008.

Kennedy, R.E., Yang, Z., Gorelick, N., Braaten, J., Cavalcante, L., Cohen, W.B., Healey, S., 2018. Implementation of the LandTrendr algorithm on Google Earth Engine. Remote Sens. 10, 1–10. https://doi.org/10.3390/rs10050691.

Lan, H., Stewart, K., Sha, Z., Xie, Y., Chang, S., 2022. Data Gap Filling Using Cloud-Based Distributed Markov Chain Tileular Automata Framework for Land Use and Land Cover Change Analysis: Inner Mongolia as a Case Study. Remote Sens. (Basel) 14 (3), 445. https://doi.org/10.3390/rs14030445.

Markham, B.L., Arvidson, T., Barsi, J.A., Choate, M., Kaita, E., Levy, R., Lubke, M., Masek, J.G., 2018. Landsat Program, in: Comprehensive Remote Sensing. Elsevier, pp. 27–90. https://doi.org/10.1016/B978-0-12-409548-9.10313-6.

Martilei, A., Mattioli, W., Puletti, N., Chianucci, F., Gianelle, D., Grotti, M., et al., 2020. Large-scale two-phase estimation of wood production by poplar plantations exploiting Sentinel-2 data as auxiliary information. SILVA FENNICA 54 (2).

Matasci, G., Hermosilla, T., Wulder, M.A., White, J.C., Coops, N.C., Hobart, G.W., Zald, H.S., 2018a. Large-area mapping of Canadian boreal forest cover, height, biomass and other structural attributes using Landsat composites and lidar plots. Remote Sens. Environ. 209, 90–106.

Matasci G., Hermosilla T., Wulder M. A., White J. C., Coops N. C., Hobart G. W., Bolton D. K., Tompalski P.,Bater C. W. 2018b. Three decades of forest structural dynamics over Canada's forested ecosystems using Landsat time-series and lidar plots. Remote Sensing of Environment Volume 216, October 2018, Pages 697-714. https://doi.org/10.1016/j.rse.2018.07.024.

Palahí, M., Valbuena, R., Senf, C., et al., 2021. Concerns about reported harvests in European forests. Nature 592, E15–E17. https://doi.org/10.1038/s41586-021-03292-x.

Pérez-Cabello, F., Montorio, F., Borini, A.D., 2021. Remote sensing techniques to assess post-fire vegetation recovery. Current Opinion in Environmental Science & Health. https://doi.org/10.1016/j.coesh.2021.100251.

Potapov, P., Hansen, M.C., Pickens, A., Hernandez-Serna, A., Tyukavina, A., Turubanova, S., Zalles, V., Li, X., Khan, A., Stolle, F., Harris, N., Song, X., Baggett, A., Kommareddy, I., Kommareddy, A., 2022. The Global 2000–2020 Land Cover and Land Use Change Dataset Derived From the Landsat Archive: First Results. Front. Remote Sens. 3, 856903 https://doi.org/10.3389/frsen.2022.856903.

Roy, D.P., Ju, J., Kline, K., Scaramuzza, P.L., Kovalskyy, V., Hansen, M., Loveland, R.T., Vermote, E., Zhang, C., 2010. Web-enabled Landsat Data (WELD): Landsat ETM+ composited mosaics of the conterminous United States. Remote Sens. Environ. https://doi.org/10.1016/j.rse.2009.08.011.

Saarinen, N., White, J., Wulder, M., Kangas, A., Tuominen, S., Kankare, V., Holopainen, M., Hyyppä, J., Vastaranta, M., 2018. Landsat archive holdings for Finland: opportunities for forest monitoring. Silva Fenn. 52 https://doi.org/10.14214/sf.9986.

Senf, C., Seidl, R., 2020. Mapping the forest disturbance regimes of Europe. Nat Sustain. https://doi.org/10.1038/s41893-020-00609-y.

Siabi, N., Hossein, S., Bijan, G.S., 2022. Effective method for filling gaps in time series of environmental remote sensing data: An example on evapotranspiration and land surface temperature images. Comput. Electron. Agric. https://doi.org/10.1016/j.compag.2021.106619.

Simonetti, D., Pimple, U., Langner, A., Marelli, A., 2021. Pan-tropical Sentinel-2 cloud-free annual composite datasets. Data Brief. https://doi.org/10.1016/j.dib.2021.107488.

Struyf, A., Hubert, M., Rousseeuw, P., 1997. Clustering in an Object-Oriented Environment. J. Stat. Softw. 1 (4), 1–30.

Summary for policy makers – State of Europe's Forests 2020. Forest Information System for Europe. https://www.eea.europa.eu/themes/biodiversity/forests/fise-the-forest-information-system.

Testa, S., Borgogno Mondino, C.E., Pedroli, C., 2014. Correcting MODIS 16-day composite NDVI time-series with actual acquisition dates. European Journal of Remote Sensing 47 (1), 285–305. https://doi.org/10.5721/EuJRS20144718.

Tuia, D., Marcos, D., Camps-Valls, G., 2016. Multi-temporal and multi-source remote sensing image classification by nonlinear relative normalization. ISPRS J. Photogramm. Remote Sens. 120, 1–12. https://doi.org/10.1016/j.isprsjprs.2016.07.004.

Vaglio, G.L., Francini, S., Luti, T., Chirici, G., Pirotti, F., Papale, D., 2021. Satellite open data to monitor forest damage caused by extreme climate-induced events: a case study of the Vaia storm in Northern Italy. Forestry: An International Journal of Forest Research 94 (3), 407–416. https://doi.org/10.1093/forestry/cpaa043.

Vaglio, G.L., Francini, S., Penna, D., Zuecco, G., Chirici, G., Berman, E., Coops, N.C., Castelli, G., Bresci, E., Preti, F., Valentini, R., 2022. SnowWarp: An open science and open data tool for daily monitoring of snow dynamics. Environmental Modelling & Software 156, 105477. https://doi.org/10.1016/j.envsoft.2022.105477.

Van doninck, J., & Tuomisto, H., 2017. Influence of Compositing Criterion and Data Availability on Pixel-Based Landsat TM/ETM+ Image Compositing Over Amazonian Forests. IEEE J. Sel. Top. Appl. Earth Obs. Remote Sens. 10 (3), 857–867.

E. Vermote, J. C. Roger, B. Franch and S. Skakun, "LaSRC (Land Surface Reflectance Code): Overview, application and validation using MODIS, VIIRS, LANDSAT and Sentinel 2 data's," IGARSS 2018 - 2018 IEEE International Geoscience and Remote Sensing Symposium, 2018, pp. 8173-8176, doi: 10.1109/IGARSS.2018.8517622.

Viana-Soto, A., Aguado, I., Salas, J., García, M., 2020. Identifying Post-Fire Recovery Trajectories and Driving Factors Using Landsat Time Series in Fire-Prone Mediterranean Pine Forests. Remote Sens. (Basel) 12 (9), 1499. https://doi.org/10.3390/rs12091499.

White, J.C., Wulder, M.A., Hobart, G.W., Luther, J.E., Hermosilla, T., Griffiths, P., Coops, N.C., Hall, R.J., Hostert, P., Dyk, A., Guindon, L., 2014. Pixel-Based Image Compositing for Large-Area Dense Time Series Applications and Science. Can. J. Remote. Sens. 40 (3), 192–212. https://doi.org/10.1080/07038992.2014.945827.

White, J.C., Wulder, M.A., Hermosilla, T., Coops, N.C., Hobart, G.W., 2017. A nationwide annual characterization of 25 years of forest disturbance and recovery for Canada using Landsat time series. Remote Sens. Environ. 194, 303–321. https://doi.org/10.1016/j.rse.2017.03.035.

Wolfe, R., Masek, J., Saleous, N., and Hall, F., "LEDAPS: mapping North American disturbance from the Landsat record," IGARSS 2004. 2004 IEEE International Geoscience and Remote Sensing Symposium, 2004, pp. 4, doi: 10.1109/IGARSS.2004.1368929.

Wulder, M., Coops, N., 2014. Satellites: Make Earth observations open access. Nature 513, 30–31. https://doi.org/10.1038/513030a.

Wulder, M.A., Masek, J.G., Cohen, W.B., Loveland, T.R., Woodcock, C.E., 2012. Opening the archive: how free data has enabled the science and monitoring promise of Landsat. Remote Sens. Environ. 122, 2–10.

Wulder, M.A., Loveland, T.R., Roy, D.P., Crawford, C.J., Masek, J.G., Woodcock, C.E., Allen, R.G., Anderson, M.C., Belward, A.S., Cohen, W.B., Dwyer, J., Erb, A., Gao, F., Griffiths, P., Helder, D., Hermosilla, T., Hipple, J.D., Hostert, P., Hughes, M.J., Huntington, J., Johnson, D.M., Kennedy, R., Kilic, A., Li, Z., Lymburner, L., McCorkel, J., Pahlevan, N., Scambos, T.A., Schaaf, C., Schott, J.R., Sheng, Y., Storey, J., Vermote, E., Vogelmann, J., White, J.C., Wynne, R.H., Zhu, Z., 2019. Current status of Landsat program, science, and applications. Remote Sens. Environ. 225, 127–147. https://doi.org/10.1016/j.rse.2019.02.015.

Wulder, M.A., Roy, D.P., Radeloff, V.C., Loveland, T.R., Anderson, M.C., Johnson, D.M., Healey, S., Zhu, Z., Scambos, T.A., Pahlevan, N., Hansen, M., Gorelick, N., Crawford, C.J., Masek, J.G., Hermosilla, T., White, J.C., Belward, A.S., Schaaf, C., Woodcock, C.E., Huntington, J.L., Lymburner, L., Hostert, P., Gao, F., Lyapustin, A., Pekel, J., Strobl, P., Cook, B.D., 2022. Fifty years of Landsat science and impacts. Remote Sens. Environ. 280, 113195 https://doi.org/10.1016/j.rse.2022.113195.

Zald, H.S.J., Wulder, M.A., White, J.C., Hilker, T., Hermosilla, T., Hobart, G.W., Coops, N.C., 2016. Integrating Landsat pixel composites and change metrics with lidar plots to predictively map forest structure and aboveground biomass in Saskatchewan. Canada. Remote Sens. Environ. 176, 188–201. https://doi.org/10.1016/j.rse.2016.01.015.

Zeng, L., Wardlow, B.D., Hu, S., Zhang, X., Zhou, G., Peng, G., Xiang, D., Wang, R., Meng, R., Wu, W., 2021. A Novel Strategy to Reconstruct NDVI Time-series with high temporal resolution from MODIS multi-temporal composite products. Remote Sens. (Basel) 13 (7), 1397. https://doi.org/10.3390/rs13071397.